Generating Attention Maps from Eye-gaze for the Diagnosis of Alzheimer's Disease

Anonymous Author(s)
Affiliation
Address
email

Abstract

Convolutional neural networks (CNNs), are currently the best computational methods for the diagnosis of Alzheimer's disease (AD) from neuroimaging. CNN's are able to automatically learn a hierarchy of spatial features, but they are not optimized to incorporate domain knowledge.

In this work we study the generation of attention maps based on a human expert gaze of the brain scans (domain knowledge) to guide the deep model to focus on the more relevant regions for AD diagnosis. Two strategies to generate the maps from eye-gaze were investigated; the use of average class maps and supervising a network to generate the attention maps. These approaches were compared with masking (hard attention) with regions of interest (ROI) and CNNs with traditional attention mechanisms.

For our experiments, we used positron emission tomography (PET) scans from the Alzheimer's Disease Neuroimaging Initiative (ADNI) database. For the task of normal control (NC) vs Alzheimer's (AD), the best performing model was with insertion of regions of interest (ROI), which achieved 95.6% accuracy, 0.4% higher than the baseline CNN.

1 Introduction

Alzheimer's Disease (AD) is a chronic brain disorder that accounts for 60% to 80% of dementia cases worldwide [1] and affects predominantly the elderly. Symptoms include forgetfulness, difficulty reasoning and mood changes like apathy, wandering, agitation and aggression. The brain presents atrophy due to death of neurons and lower metabolic activity. While there is still no cure for AD, its early detection is crucial, as an effective management of the disease may help prevent the progression to more severe stages. Clinical diagnosis is made by collecting medical and family history, asking relatives about changes in behaviour and conducting mental cognitive tests. Brain imaging, like magnetic resonance imaging (MRI) scans or positron emission tomography (PET) scans has also been recognized as a powerful biomarker, however their interpretation is difficult thus computer-aided diagnosis (CAD) has been requested by clinicians to amplify their diagnostic accuracy [2].

Currently, the best performing algorithms for AD classification from neuroimaging are convolutional neural networks (CNNs). In these networks, the features are automatically extracted rather than handcrafted, however it is not easy to incorporate medical knowledge.

A recent survey on deep models for medical image analysis concluded that integrating domain knowledge improved the performance of the networks in almost all tasks [3]. As an example, it states that the attention mechanism is a powerful technique to incorporate domain knowledge of radiologists, because the information about where medical doctors focus helped deep learning models yield better results [4] [5] [6] [7] [8] [9]. Inspired by these results, in this work we investigate

Submitted to 36th Conference on Neural Information Processing Systems (NeurIPS 2022). Do not distribute.

whether the generation of attention maps based on eye-tracking data (physician gaze) can improve the performance of AD diagnosis, by directing the classification model to focus on important regions (determined by domain knowledge). The maps that are obtained are multiplied with CNN feature maps, thus certain locations are highlighted while others are attenuated. Two approaches were investigated for attention map generation. In the first approach, average maps are computed from the doctor's gaze maps for patients of the same class. In the second approach, the eye-gaze data is used to supervise a CNN trained to generate attention maps. The inferred maps, like in the first approach, are then multiplied with the feature maps of the CNN that does classification, and whose parameters are trained with the class labels only. Finally, this CNN was also trained with regions of interest (ROI) to compare intuitive domain knowledge with pre-defined relevant regions for classification.

Therefore, the main contributions of this work are:

- Introduction of domain knowledge from eye-gaze data from an expert physician into a state-of-the-art CNN model to perform AD classification.
- Training a deep multiscale network network and a U-Net with physician eye-gaze data to predict attention maps.

2 Related Work

2.1 AD detection models

In the last decade, there have been substantial developments in machine learning classification models for AD detection. CNNs are very effective for AD classification problems and ResNets are by far the most popular type of CNN applied [10] [11] [12] [13] [14] [15] [16]. Nonetheless, some authors used AlexNet [17], Inception [18] and VGG [19] [20] or applied an ensemble of methods [21]. Most studies train models with magnetic resonance imaging (MRI) scans [10] [11] [22] [12] [13] [14] [23] [20] [15] [16], although still a considerable number use other biomarkers, like PET scans [24] [17] [25] [21] [18] [26] [27] [19], largely from the Alzheimer's Disease Neuroimaging Initiative (ADNI) clinical datasets.

A recent in-depth study [28] about deep learning applications in AD diagnosis research analyzed about 100 published papers since 2019. Besides identifying many trending technologies, the study recognized the importance of the attention mechanism (AM) and suggested it should be further explored. The idea behind the attention mechanism comes from human visual attention, which illustrates that human vision typically does not scan the entire scene at once, but rather focuses on selective parts of the whole visual field sequentially, according to the person's needs. The AM therefore can be interpreted as weighted values that represent the importance of each specific part of the image for classification. In CNN models there can be many types of attention, like spatial attention, channel attention, self-attention and layer attention, all of which were employed in the analyzed papers. As for examples of models, Dan J. et al. [11] trained a 3D ResNet with one layer of spatial attention (convolution and rectified linear unit (ReLU)), which led to an increase of 2% in accuracy. Ullanant et al. [12] inserted a residual attention block [29] to a vanilla ResNet. Liang S et al.[13] used one layer of channel attention per stage. Each attention block has global max-pooling for each channel, a convolution with 1x1 kernel, ReLU and dense layers. Zhang Y. et al.[15], created an attention mechanism inspired by the Squeeze-and-Excitation block [30] (channel attention) and got an increase of about 2% in accuracy. Regarding the location of the attention mechanism in the network, most studies place it in the middle of the network or throughout every residual block. However, one author [31] concluded the AM was better placed at the head of the network.

All of the experiments mentioned that used AM were made with MRI scans. No studies that applied attention mechanisms to PET scans were found. Nonetheless, PET scans were chosen for this work, because they can show brain alterations before anatomical changes are observed in MRI scans, which is important for early diagnosis [32].

2.2 Supervised attention

Since there were no studies on the effect of supervising attention mechanisms with human gaze (domain knowledge) for Alzheimer's disease, we looked at works in other fields.

Table 1: Clinical profile of the subjects in three categories (AD, MCI, NC) categories. Age and MMSE are average values with the standard deviation in parenthesis. MMSE refers to the Mini-Mental State Exam, a mental cognitive status assessment that evaluates memory, thinking and simple problem-solving abilities, where the maximum (best) score is 30.

Group	AD	MCI	NC	All
No. of subjects	95	207	104	406
Age	76.6 (7.1)	76.0 (7.3)	77.0 (4.8)	76.4 (6.7)
Sex (% M)	59.9	65.8	63.8	64.1
MMSE	21.1 (4.1)	26.7 (2.8)	29.1 (1.2)	26.1 (2.9)

Yu et al. [33] showed that spatial attention guided by human eye-tracking data can, in fact, enhance performance, in their case, the performance of generating short text information about brief video clips. They created an AM block that predicts a gaze map per frame of the input video. the inclusion of this AM block improved the results by 3.2% for one language metric.

Li et al. [4] proposed a CNN for glaucoma detection with an attention mechanism supervised by human attention, called AG-CNN. The human-generated attention maps were used to train the attention prediction subnet of their AG-CNN, which is comprised of a CNN with concatenated features of different layers passed through a deconvolution block at the end. Li's model has considerably better performance than other state-of-the-art methods in his field and increased accuracy by 3.4% when compared to the same model without attention.

Chong Ma et al. [34] proposed a vision transformer for the diagnosis of breast diseases. They infuse the human expert's prior knowledge to guide the network to focus on the patches with potential pathology. This design leads to higher performance (increased accuracy by almost 1% compared to a standard ResNet50). Moreover, the EG-ViT only introduces the mask operation and an additional residual connection to a vanilla vision transformer. This model has the limitation that it needs to be pre-trained with hundreds of millions of data samples in order to show better results than CNN. This is especially troublesome for 3D images.

Sheng Wang et al. [35] designed a supervised network to assess knee X-ray images for osteoarthritis. This model, called GA-Net, is composed of a ResNet classification network and the supervised attention consistency block. This last component is a CAM visualization/localization module [36]. Comparing the ResNet18 with ResNet18+Gaze, the accuracy increased by 2% to 62.8%.

3 Data

ADNI is a landmark partnership with the purpose of creating a longitudinal study intended to collect biomarkers of AD. From this database, we retrieved fludeoxyglucose (FDG) PET scans, which show the glucose metabolism in the brain, from participants with baseline and 6, 12 and 24-month follow-ups. 1393 scans from 209 subjects were used, 95 were from AD subjects, 207 were from mild cognitive impairment (MCI) subjects and 104 were normal controls (NC). Tab 1 presents demographic and clinical information of the study subjects. All FDG-PET had been normalized, averaged and co-registered by ADNI, and were also further normalized to the [0,1] range.

Additionally, several PET scan images in this dataset have been complemented with records of the gaze of a medical doctor while performing a diagnosis, thus collecting areas of interest (domain knowledge). This was performed by Bicacro et al. [37], using a Tobii™ device. For their study, the gaze (a total of 4261 fixation points) for scans of 177 subjects (59 of each category - AD, MCI, NC) was collected. Tab. 2 presents the proportion of each type of scan within the overall dataset. It is noteworthy that the amount of scans with fixations is only 12.6% of the total scans available. Even though these eye-gaze data have been applied before in [37] and [38], it was never employed in deep learning models. They were used for selecting and extracting features that were then fed to a support vector machine classifier.

For each scan, the eye-tracker provides discrete fixation points. However, the physician does not look at a particular pixel, but instead looks at a region centered in the fixation point and symmetrically

Table 2: PET scans in various categories. Several different scans correspond to the same patients in different periods of the ADNI's longitudinal study, therefore there are more scans than subjects.

Group	AD	MCI	NC	All
No. of scans	314	714	365	1393
Proportion of total (%)	22.5	51.2	26.3	100
Proportion of scans with fixations (%)	4.2	4.2	4.2	12.6

spread out by the visual angle. Therefore, we convolve the fixation map $f(x)$ (image with the points where the doctor focused) with an isotropic bi-dimensional Gaussian function $G_\sigma(x)$, creating an attention map $S(x)$, like in Fig. 1 ((a), (b), (c)) (image where the regions people's eyes focus are highlighted). The circular region is modeled by the isotropic Gaussian filter and the visual angle by the standard deviation ($\sigma = 3$). Some examples of the resulting maps are shown in Fig. 1, where average maps are also shown ((d), (e), (f)), given the variability in attention maps.

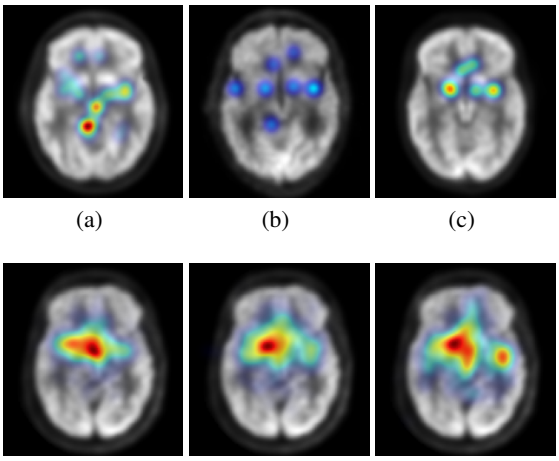

(a) (b) (c)

(d) (e) (f)

Figure 1: Examples of axial cut 25. The first row shows attention maps obtained by Gaussian filtering of the fixation points for three random patients, with NC (a), MCI (b) and AD (c). The second row shows average attention maps for NC (d), MCI (e) and AD (f).

The same expert physician has manually identified 12 regions of interest (ROI), as displayed in Fig. 2. These regions include the lateral and mesial temporal, inferior frontal gyrus/orbitofrontal, inferior and superior anterior cingulate, dorsolateral parietal, posterior cingulate, and precuneus. These anatomical regions of the brain are considered by the doctor to be the most relevant for the task of AD diagnosis. If we compare the regions of interest with the regions where the doctor looked at, we discover that only 36.2% of fixations fall inside the ROI. This might be concerning since it seems there is little coherence between the regions identified by the doctor and the regions where he focuses his gaze.

4 Method

In this section, the different models studied are detailed. First, we present the two models investigated for attention mechanism supervision, then we present our approaches that use constant attention maps, either based on average eye-gaze data or from ROIs. Finally, we present our baselines which include a standard ResNet18 and the ResNet18 with attention mechanisms (either CBAM or Residual Attention).

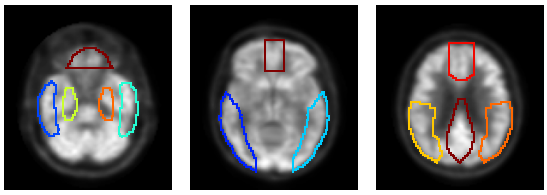

(a) (b) (c)

Figure 2: Examples of three axial slices with regions of interest (ROI) defined by the expert physician. (a) Red - Inferior frontal gyrus/Orbitofrontal; Dark and light blue - Lateral temporal; Light green and orange - Mesial temporal; (b) Dark and light blue - Lateral temporal; Red - Inferior and superiro anterior cingulate ; (c) Light red - Inferior and superior anterior cingulate ; Yellow and orange - Dorsolateral parietal; Dark red - Posterior cingulate and precuneus. Some slices do not contain any anatomical ROI.

4.1 Supervised attention mechanism

In this method, the model is composed of two sub-networks. The first network is used to predict the attention maps, and is supervised by the doctor's fixation maps. The second network is a standard ResNet18, where the created attention mechanism maps are inserted. Two alternatives for generating the attention maps from the doctors' eye-gaze were investigated. The first alternative is the deep multiscale network (Fig. 3), which is similar to the glaucoma paper's [4] attention prediction subnet, but adapted for 3D images and with resizing performed with average pooling and upsampling instead of bilinear interpolation. The encoder portion is a typical CNN, where the input passes through several residual blocks to extract hierarchical features. The decoder portion takes features from distinct basic blocks, normalizes them to the same dimensions, and concatenates them to perform convolutions four times, before applying convolution transpose twice.

The second alternative is a U-Net (Fig. 4), which is also an encoder-decoder network. The encoder part performs feature extraction and learns abstract representations of the input image with convolutions. Here, the spatial dimensions decrease with max pooling operations. Furthermore, the network has two skip connections between the encoder and decoder part, that concatenates two arrays, to be used in the next decoder stage. This helps to provide additional information to the decoder and assists in the flow of the gradient while backpropagating, since it is a shortcut. The decoder section takes the representations to generate the mask. It increases the size through upsampling.

4.2 Constant average maps and ROI

In this approach, the attention maps are not created by layers with learned weights. Instead, the doctor's constant average attention map for each class (based on the eye-tracking data) and the ROI maps (hard attention) are introduced into the network, without learning. These maps are inserted in the ResNet18 in the same place as the CBAM module.

4.3 Baseline CNNs

The simplest baseline is a vanilla 3D ResNet18. This is an appropriate model since residual networks are considered state-of-the-art and have been widely applied for AD classification. In fact, 38% of the 74 papers that used CNNs for AD diagnosis analyzed by Khojaste-Sarakhsi et al. used ResNets [28]. Although this network does not include attention, we can visualize the regions of the input scans that the model considers more important with guided back-propagation [39] or Grad-CAM [40].

Two additional baselines were tested, which integrated attention mechanisms into the ResNet, but that do not incorporate domain knowledge. One attention mechanism is CBAM [41], a commonly used attention module that can be integrated into any CNN. CBAM sequentially infers attention maps along two separate dimensions, channel and spatial, which are multiplied by the input of the respective layer creating a refined feature map. For this study, CBAM was adapted for three dimensions, the same as the scans. To better understand the importance of the spatial attention component, the experiments were also done with the spatial attention sub-module only. The CBAM block was inserted in three

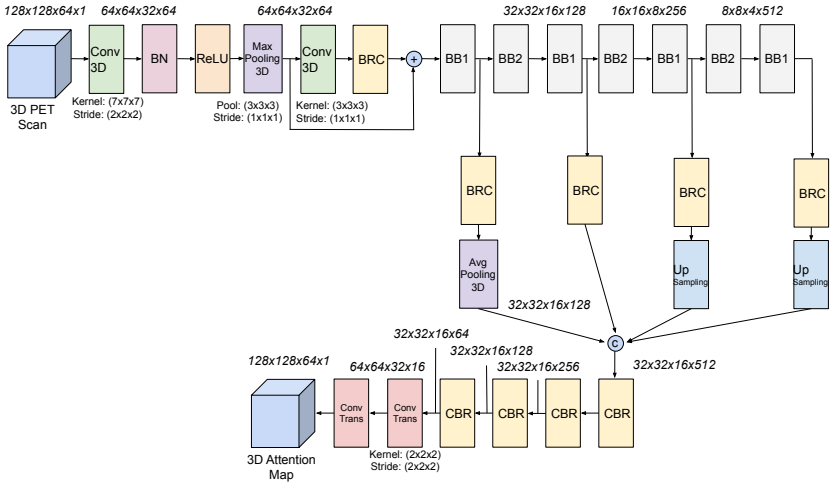

Figure 3: Representation of deep multiscale network that was chosen to learn the attention maps. BRC means batch normalization, ReLU and convolution layers.

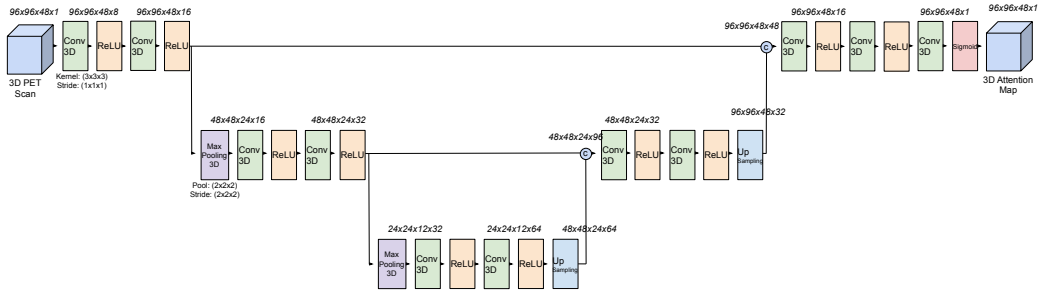

Figure 4: Representation of a 3D U-Net, the second network investigated for AM generation with eye-gaze supervision.

different locations (one per trial): at the start of the network before any operation, in the middle basic block, and throughout the basic blocks of the ResNet.

Another attention mechanism tested is residual attention [29]. This is another type of spatial and channel attention. It uses a bottom-up top-down structure to learn the mask. It collects global information and later guides input features in each position.

4.4 Experimental setup

The baseline CNN, the ResNets with CBAM and residual attention and the networks with constant maps/ROI were trained with categorical cross-entropy as the loss function, which was minimized with stochastic gradient descent optimizer for a maximum of 50 epochs. The learning rate was 1×10^{-2}. Train and testing were done using stratified 5-fold cross-validation. Since we have multiple scans of the same subject at different times, the subjects, and not the images, were separated into five folds. This methodology guarantees that brain scans from the same subject are not present in different sets, thus avoiding data leakage. About 15% of the available samples for training in each fold were used for validation. The model of the epoch with the lowest validation loss was selected as the best model to be tested. The supervised attention mechanism networks (deep multiscale network and U-Net) were trained like the aforementioned models but with Dice coefficient as loss. All models were created with the keras/Tensorflow package on Google Colab notebooks. The main components can be

Table 3: Results of 5 fold cross validation for the task NC vs AD. Format: Mean (standard deviation), best result in bold. The lower section consists of models with domain knowledge, while the upper section does not. All the models are composed of a ResNet18 and the AM module specified in the first column.

Models	AM Location	ACC (%)	SEN (%)	SPE (%)	F_1-score (%)
Standard ResNet18	-	95.2 (1.7)	95.0 (2.4)	95.3 (2.4)	94.8 (1.9)
CBAM	middle	94.9 (2.0)	94.7 (2.7)	95.3 (2.7)	94.6 (2.4)
CBAM spatial module	middle	95.0 (1.7)	94.8 (3.1)	95.2 (3.4)	94.6 (2.4)
Residual attention	throughout	95.5 (2.2)	94.7 (3.8)	**96.2 (2.3)**	94.8 (2.4)
Constant average map	middle	94.8 (1.5)	93.7 (3.4)	95.9 (2.4)	94.4 (1.5)
ROI	start	**95.6 (2.6)**	**95.1 (2.5)**	96.1 (2.8)	**95.2 (2.7)**
Deep multiscale network	start	94.0 (1.9)	92.9 (4.0)	94.9 (2.4)	93.4 (2.8)
U-Net	middle	95.2 (2.1)	94.7 (4.0)	95.6 (2.2)	94.6 (2.1)

found in this link: `https://tinyurl.com/GitHubPaperCode`. The classification tasks performed were NC vs AD and NC vs MCI vs AD.

5 Results and discussion

The results (accuracy, sensitivity, specificity and F_1-score) for the task NC vs AD and NC vs MCI vs AD are displayed in Tab. 3 and Tab. 4, respectively. All the models include a ResNet18. The tables only show the results for the best location of the attention mechanism (start, middle or throughout the network), as specified in the 'AM Location' column. The statistical significance of the differences between the results of each AM strategy and the baseline Resnet were evaluated with paired t-test Wilcoxon tests.

For NC vs AD, the model with the highest accuracy was ResNet18 with ROI inserted in the start, achieving 95.6% accuracy. This was a 0.4% rise compared to the standard ResNet18, which is statistically significant (p-value<0.05), and the best performing model with domain knowledge.

Fig. 5 displays a brain scan overlapped with heatmaps generated by guided backpropagation (a) and Grad-CAM (b) techniques of the standard ResNet18, as well as a scan with fixation points and ROI (c) for comparison. The red areas mean these regions are more important for the classification task. The most important regions for the guided backpropagation mode are slightly different than the ones activated by the Grad-CAM method, except for the center of the brain, which has some red regions for both types of images. The Grad-CAM maps are more similar to the doctor fixations than to the ROI. Nonetheless, from these types of images, no indisputable pattern stands out as a determinate location of the disease.

Examples of the generated attention maps are presented in Fig. 6. We computed the Pearson correlation between these maps and the original fixation maps (results not shown) and concluded that the deep multiscale Net created maps more similar to the original than the U-Net. Despite this, the U-net obtained slightly better performance and was the best method that incorporated the doctor's attention. Nevertheless, it was not able to obtain better performance than the baselines (p-values<0.05). Some reasons can be hypothesized: the eye-gaze dataset was too small, specially for deep learning which needs a lot of data; the methods of incorporating the eye-gaze were not the most suitable (other approaches were suggested, for example, a supervised CAM module [35] or a vision transformer with domain data [34]); the assumption that the doctor relies only on the intensity of the voxels to make decisions may be very simplistic, perhaps the doctor is comparing different regions' average intensity, performing basic computations or the mental process of information is different according to the region being analyzed.

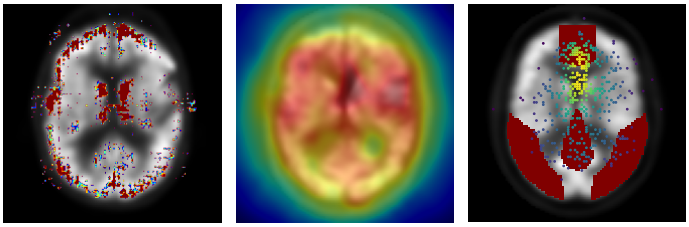

(a) (b) (c)

Figure 5: Examples of localization maps using Guided Backpropagation (a) and Grad-CAM (b) techniques for the standard ResNet18 for the task NC vs AD. Each of the maps presented is an average of the generated guided backpropagation and Grad-CAM output for all AD scans available. These maps highlight the regions of the brain image more activated in the network to make the prediction. (c) ROI and fixation points are displayed for comparison.

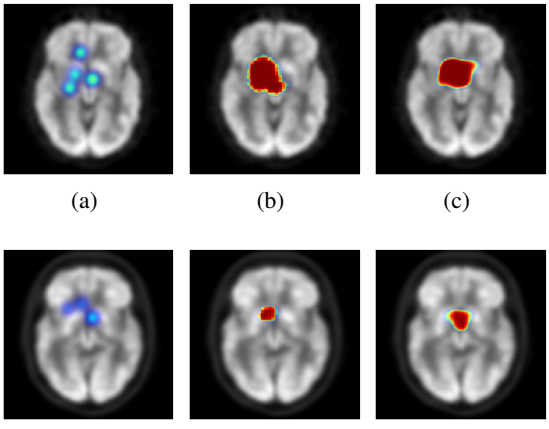

(a) (b) (c)

(d) (e) (f)

Figure 6: Examples of generated attention maps for axial cut 25 (first row - AD; second row - MCI). The doctor fixation maps are on the left, the deep multiscale network generated attention maps are in the middle and the U-Net maps on the right.

For the task NC vs MCI vs AD, the best performing model is the ResNet18 with a constant average duration map in the middle, with 87.4% accuracy (+0.3% than standard ResNet18 and p-value<0.05). This means a different conclusion than for the task NC vs AD, for which the best performing model was with ROI. Therefore, perhaps the ROIs are optimized for AD regions and do not take into account MCI, while the eye-gaze was retrieved when the doctor was performing a classification task that included MCI (NC vs MCI vs AD), thus the constant average maps include this information.

The accuracy results of incorporating the CBAM spatial model and residual attention were not statistically different from those in the baseline ResNet for the binary task, but were statistically significant for the ternary task.

Fig. 7 shows the accuracy of our models (in green) juxtaposed with the state-of-the-art networks for better comparison (in gray and blue). This figure shows that our deep models outperformed the studies found in the literature. Yet, these comparisons need to be taken lightly because different models were trained, with different biomarkers and with a different number of scans. The figure also highlights that incorporating domain knowledge helped increase accuracy with ROI for the binary task and constant average maps for the multiclass task.

Our methods also performed better than most expert physicians in NC vs AD classification, who correctly predict 85.7% of scans on average [42]

Table 4: Results of 5 fold cross validation for the task NC vs MCI vs AD. Format: Mean (standard deviation), best result in bold. All the models are composed of a ResNet18 and the AM module specified in the first column.

Models	AM Location	ACC (%)	F_1-score (%)
Standard ResNet18	-	87.1 (1.6)	86.0 (1.8)
CBAM	middle	85.9 (1.6)	84.2 (3.0)
CBAM spatial module	middle	86.9 (2.0)	**86.8 (2.3)**
Residual attention	throughout	85.5 (0.9)	82.0 (3.8)
Constant average map	middle	**87.4 (1.5)**	85.4 (3.4)
ROI	start	86.2 (1.4)	86.6 (1.4)
Deep multiscale network	start	86.6 (2.3)	85.8 (1.6)
U-Net	middle	86.0 (2.3)	85.2 (1.6)

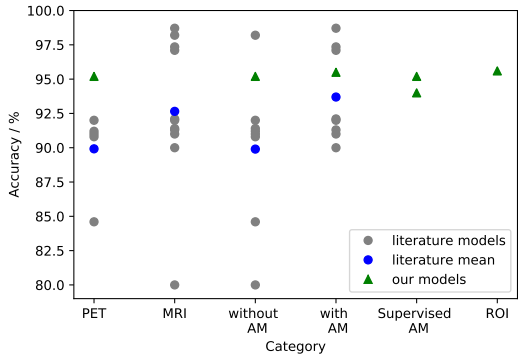

Figure 7: Comparison with state-of-the-art, for the task NC vs AD. Accuracy of our models (in green) contrasted with the models reviewed (in gray) and with the average value of the state-of-the-art models (in blue). 'PET' denotes models trained with PET scans only; 'MRI' denotes models trained with MRI scans only; 'without AM' denotes models without attention mechanism; 'with AM' denotes models that use attention mechanism; 'Supervised AM' refers to our models with supervised attention mechanism (there are no other state-of-the-art models in this category). Finally, on the right, the model with ROI, which was the best performing model.

6 Conclusion

In this work we investigated methods to integrate physician attention patterns obtained from eye-tracking data into CNNs for Alzheimer's Disease diagnosis. We explored the use of average gaze-maps and the supervision of a CNN to predict attention maps. We also compared these approaches with the use of ROI hard attention maps.

Our methods performed better than most CAD systems for AD working with FDG-PET images found in the literature. The ResNet18 with the ROI yielded the best results for NC vs AD, with an accuracy of 95.6% and the ResNet18 with constant average maps (Gaussian filtered eye gaze) achieved 87.4% for NC vs MCI vs AD task. These outcomes motivate further work like the creation of a bigger dataset, with more gaze data, following other approaches of introducing domain knowledge, like the visual transformer [34] or a CAM module [35] and extracting more information from the data besides just the voxel intensity of the "looked at" regions.

References

[1] J. Gaugler, B. James, T. Johnson, A. Marin, and J. Weuve, "2020 Alzheimer's Disease facts and figures," *Alzheimer's and Dementia*, vol. 16, pp. 391–460, 2020.

[2] S. Gauthier, P. Rosa-Neto, J. A. Morais, and C. Webster, "World Alzheimer Report 2021: Journey through the diagnosis of dementia," Alzheimer's Disease International, Tech. Rep., 2021.

[3] X. Xie, J. Niu, X. Liu, Z. Chen, S. Tang, and S. Yu, "A survey on incorporating domain knowledge into deep learning for medical image analysis," *Medical Image Analysis*, vol. 69, p. 101985, 2021. [Online]. Available: https://www.sciencedirect.com/science/article/pii/S1361841521000311

[4] L. Li, M. Xu, H. Liu, Y. Li, X. Wang, L. Jiang, Z. Wang, X. Fan, and N. Wang, "A Large-Scale Database and a CNN Model for Attention-Based Glaucoma Detection," *IEEE Transactions on Medical Imaging*, vol. 39, no. 2, pp. 413–424, 2020.

[5] M. Mitsuhara, H. Fukui, Y. Sakashita, T. Ogata, T. Hirakawa, T. Yamashita, and H. Fujiyoshi, "Embedding Human Knowledge in Deep Neural Network via Attention Map," in *VISIGRAPP*, 2021.

[6] L. Fang, C. Wang, S. Li, H. Rabbani, X. Chen, and Z. Liu, "Attention to Lesion: Lesion-Aware Convolutional Neural Network for Retinal Optical Coherence Tomography Image Classification," *IEEE Transactions on Medical Imaging*, vol. 38, no. 8, pp. 1959–1970, 2019.

[7] H. Cui, Y. Xu, W. Li, L. Wang, and H. Duh, "Collaborative Learning of Cross-Channel Clinical Attention for Radiotherapy-Related Esophageal Fistula Prediction from CT," in *Medical Image Computing and Computer Assisted Intervention – MICCAI 2020: 23rd International Conference, Lima, Peru, October 4–8, 2020, Proceedings, Part I*. Berlin, Heidelberg: Springer-Verlag, 2020, p. 212–220. [Online]. Available: https://doi.org/10.1007/978-3-030-59710-8_21

[8] X.-Z. Xie, J.-W. Niu, X.-F. Liu, Q.-F. Li, Y. Wang, J. Han, and S. Tang, "DG-CNN: Introducing Margin Information into Convolutional Neural Networks for Breast Cancer Diagnosis in Ultrasound Images," *Journal of Computer Science and Technology*, vol. 37, no. 2, p. 277, 2022. [Online]. Available: https://jcst.ict.ac.cn/EN/abstract/article_2863.shtml

[9] B. Zhang, Z. Wang, J. Gao, C. Rutjes, K. Nufer, D. Tao, D. D. Feng, and S. W. Menzies, "Short-Term Lesion Change Detection for Melanoma Screening With Novel Siamese Neural Network," *IEEE Transactions on Medical Imaging*, vol. 40, no. 3, pp. 840–851, 2021.

[10] S. Korolev, A. Safiullin, M. Belyaev, and Y. Dodonova, "Residual and plain convolutional neural networks for 3D brain MRI classification," in *2017 IEEE 14th International Symposium on Biomedical Imaging (ISBI 2017)*, 2017, pp. 835–838.

[11] D. Jin, J. Xu, K. Zhao, F. Hu, Z. Yang, B. Liu, T. Jiang, and Y. Liu, "Attention-based 3D Convolutional Network for Alzheimer's Disease Diagnosis and Biomarkers Exploration," in *2019 IEEE 16th International Symposium on Biomedical Imaging (ISBI 2019)*, 2019, pp. 1047–1051.

[12] V. Ullanat, V. Balamurali, and A. Rao, "A Novel Residual 3-D Convolutional Network for Alzheimer's disease diagnosis based on raw MRI scans," in *2020 IEEE-EMBS Conference on Biomedical Engineering and Sciences (IECBES)*, 2021, pp. 82–87.

[13] S. Liang and Y. Gu, "Computer-Aided Diagnosis of Alzheimer's Disease through Weak Supervision Deep Learning Framework with Attention Mechanism," *Sensors*, vol. 21, no. 1, 2021. [Online]. Available: https://www.mdpi.com/1424-8220/21/1/220

[14] X. Zhang, L. Han, W. Zhu, L. Sun, and D. Zhang, "An Explainable 3D Residual Self-Attention Deep Neural Network for Joint Atrophy Localization and Alzheimer's Disease Diagnosis using Structural MRI," *IEEE Journal of Biomedical and Health Informatics*, 2021. [Online]. Available: http://dx.doi.org/10.1109/JBHI.2021.3066832

[15] Y. Zhang, Q. Teng, Y. Liu, Y. Liu, and X. He, "Diagnosis of Alzheimer's Disease Based on Regional Attention with sMRI Gray Matter Slices," *Journal of Neuroscience Methods*, p. 109376, 2021. [Online]. Available: https://www.sciencedirect.com/science/article/pii/S0165027021003113

[16] H. Sun, A. Wang, W. Wang, and C. Liu, "An improved deep residual network prediction model for the early diagnosis of Alzheimer's disease," *Sensors*, vol. 21, 6 2021.

[17] C. Zheng, Y. Xia, Y. Chen, X. Yin, and Y. Zhang, "Early Diagnosis of Alzheimer's Disease by Ensemble Deep Learning Using FDG-PET," in *Lecture Notes in Computer Science*. Springer International Publishing, 2018, pp. 614–622. [Online]. Available: https://doi.org/10.1007/978-3-030-02698-1_53

[18] Y. Ding, J. H. Sohn, M. G. Kawczynski, H. Trivedi, R. Harnish, N. W. Jenkins, D. Lituiev, T. P. Copeland, M. S. Aboian, C. Mari Aparici, S. C. Behr, R. R. Flavell, S.-Y. Huang, K. A. Zalocusky, L. Nardo, Y. Seo, R. A. Hawkins, M. Hernandez Pampaloni, D. Hadley, and B. L. Franc, "A deep learning model to predict a diagnosis of Alzheimer disease by using 18F-FDG PET of the brain," *Radiology*, vol. 290, no. 2, pp. 456–464, Feb. 2019.

[19] S.-Y. Lee, H. Kang, J.-H. Jeong, and D.-y. Kang, "Performance evaluation in [18F]Florbetaben brain PET images classification using 3D Convolutional Neural Network," *PLOS ONE*, vol. 16, no. 10, pp. 1–16, 10 2021. [Online]. Available: https://doi.org/10.1371/journal.pone.0258214

[20] Y. Turkan and F. B. Tek, "Convolutional Attention Network for MRI-based Alzheimer's Disease Classification and its Interpretability Analysis," *2021 6th International Conference on Computer Science and Engineering (UBMK)*, pp. 1–6, 9 2021. [Online]. Available: https://ieeexplore.ieee.org/document/9558882/

[21] M. Liu, D. Cheng, and W. Yan, "Classification of Alzheimer's Disease by Combination of Convolutional and Recurrent Neural Networks Using FDG-PET Images," *Frontiers in Neuroinformatics*, vol. 12, 2018. [Online]. Available: https://www.frontiersin.org/article/10.3389/fninf.2018.00035

[22] S. Basaia, F. Agosta, L. Wagner, E. Canu, G. Magnani, R. Santangelo, and M. Filippi, "Automated classification of Alzheimer's disease and mild cognitive impairment using a single MRI and deep neural networks," *NeuroImage: Clinical*, vol. 21, p. 101645, 2019. [Online]. Available: https://www.sciencedirect.com/science/article/pii/S2213158218303930

[23] J. Zhang, B. Zheng, A. Gao, X. Feng, D. Liang, and X. Long, "A 3D densely connected convolution neural network with connection-wise attention mechanism for Alzheimer's disease classification," *Magnetic Resonance Imaging*, vol. 78, pp. 119–126, 5 2021.

[24] S. Singh, A. Srivastava, L. Mi, K. Chen, Y. Wang, R. J. Caselli, D. Goradia, and E. M. Reiman, "Deep-learning-based classification of FDG-PET data for Alzheimer's disease categories," in *13th International Conference on Medical Information Processing and Analysis*, J. Brieva, J. D. García, N. Lepore, and E. Romero, Eds. SPIE, Nov. 2017.

[25] D. Lu, , K. Popuri, G. W. Ding, R. Balachandar, and M. F. Beg, "Multimodal and Multiscale Deep Neural Networks for the Early Diagnosis of Alzheimer's Disease using structural MR and FDG-PET images," *Scientific Reports*, vol. 8, no. 1, Apr. 2018. [Online]. Available: https://doi.org/10.1038/s41598-018-22871-z

[26] T. Jo, , K. Nho, S. L. Risacher, and A. J. Saykin, "Deep learning detection of informative features in tau PET for Alzheimer's disease classification," *BMC Bioinformatics*, vol. 21, no. S21, Dec. 2020. [Online]. Available: https://doi.org/10.1186/s12859-020-03848-0

[27] H. Choi, Y. K. Kim, E. J. Yoon, J.-Y. Lee, D. S. Lee, and Alzheimer's Disease Neuroimaging Initiative, "Cognitive signature of brain FDG-PET based on deep learning: domain transfer from Alzheimer's disease to Parkinson's disease," *Eur. J. Nucl. Med. Mol. Imaging*, vol. 47, no. 2, pp. 403–412, Feb. 2020.

[28] M. Khojaste-Sarakhsi, S. S. Haghighi, S. F. Ghomi, and E. Marchiori, "Deep learning for Alzheimer's disease diagnosis: A survey," *Artificial Intelligence in Medicine*, vol. 130, p. 102332, 2022. [Online]. Available: https://www.sciencedirect.com/science/article/pii/S0933365722000975

[29] F. Wang, M. Jiang, C. Qian, S. Yang, C. Li, H. Zhang, X. Wang, and X. Tang, "Residual Attention Network for Image Classification," in *2017 IEEE Conference on Computer Vision and Pattern Recognition (CVPR)*, 2017, pp. 6450–6458.

[30] J. Hu, L. Shen, and G. Sun, "Squeeze-and-Excitation Networks," in *2018 IEEE/CVF Conference on Computer Vision and Pattern Recognition*, 2018, pp. 7132–7141.

[31] M. Zheng, J. Xu, Y. Shen, C. Tian, J. Li, L. Fei, M. Zong, and X. Liu, "Attention-based CNNs for Image Classification: A Survey," *Journal of Physics: Conference Series*, vol. 2171, no. 1, p. 012068, jan 2022. [Online]. Available: https://doi.org/10.1088/1742-6596/2171/1/012068

[32] D. V. Mayblyum, J. A. Becker, H. I. L. Jacobs, R. F. Buckley, A. P. Schultz, J. Sepulcre, J. S. Sanchez, Z. B. Rubinstein, S. R. Katz, K. A. Moody, P. Vannini, K. V. Papp, D. M. Rentz, J. C. Price, R. A. Sperling, K. A. Johnson, and B. J. Hanseeuw, "Comparing PET and MRI biomarkers predicting cognitive decline in preclinical Alzheimer's disease," *Neurology*, vol. 96, no. 24, pp. e2933–e2943, May 2021.

[33] Y. Yu, J. Choi, Y. Kim, K. Yoo, S.-H. Lee, and G. Kim, "Supervising Neural Attention Models for Video Captioning by Human Gaze Data," in *2017 IEEE Conference on Computer Vision and Pattern Recognition (CVPR)*, 2017, pp. 6119–6127.

[34] C. Ma, L. Zhao, Y. Chen, L. Zhang, Z. Xiao, H. Dai, D. Liu, Z. Wu, Z. Liu, S. Wang, J. Gao, C. Li, X. Jiang, T. Zhang, Q. Wang, D. Shen, D. Zhu, and T. Liu, "Eye-gaze-guided Vision Transformer for Rectifying Shortcut Learning," 2022. [Online]. Available: https://arxiv.org/abs/2205.12466

[35] S. Wang, X. Ouyang, T. Liu, Q. Wang, and D. Shen, "Follow My Eye: Using Gaze to Supervise Computer-Aided Diagnosis," *IEEE Transactions on Medical Imaging*, pp. 1–1, 2022.

[36] B. Zhou, A. Khosla, A. Lapedriza, A. Oliva, and A. Torralba, "Learning Deep Features for Discriminative Localization," in *2016 IEEE Conference on Computer Vision and Pattern Recognition (CVPR)*, 2016, pp. 2921–2929.

[37] E. Bicacro, M. Silveira, J. S. Marques, and D. C. Costa, "3D brain image-based diagnosis of Alzheimer's disease: Bringing medical vision into feature selection," in *2012 9th IEEE International Symposium on Biomedical Imaging (ISBI)*, 2012, pp. 134–137.

[38] P. Morgado, M. C. da Silveira, and J. S. Marques, "Automated Diagnosis of Alzheimer's Disease using PET Images: A study of alternative procedures for feature extraction and selection," Master's thesis, Instituto Superior Técnico, 9 2012.

[39] J. T. Springenberg, A. Dosovitskiy, T. Brox, and M. Riedmiller, "Striving for Simplicity: The All Convolutional Net," 2014. [Online]. Available: https://arxiv.org/abs/1412.6806

[40] R. R. Selvaraju, M. Cogswell, A. Das, R. Vedantam, D. Parikh, and D. Batra, "Grad-CAM: Visual Explanations from Deep Networks via Gradient-Based Localization," in *2017 IEEE International Conference on Computer Vision (ICCV)*, 2017, pp. 618–626.

[41] S. Woo, J. Park, J.-Y. Lee, and I. S. Kweon, "CBAM: Convolutional Block Attention Module," in *Computer Vision – ECCV 2018*, V. Ferrari, M. Hebert, C. Sminchisescu, and Y. Weiss, Eds. Cham: Springer International Publishing, 2018, pp. 3–19.

[42] S. Klöppel, C. M. Stonnington, J. Barnes, F. Chen, C. Chu, C. D. Good, I. Mader, L. A. Mitchell, A. C. Patel, C. C. Roberts, N. C. Fox, J. Jack, Clifford R., J. Ashburner, and R. S. J. Frackowiak, "Accuracy of dementia diagnosis—a direct comparison between radiologists and a computerized method," *Brain*, vol. 131, no. 11, pp. 2969–2974, 10 2008. [Online]. Available: https://doi.org/10.1093/brain/awn239

Checklist

1. For all authors...
   (a) Do the main claims made in the abstract and introduction accurately reflect the paper's contributions and scope? [Yes]
   (b) Did you describe the limitations of your work? [Yes] See section 5.
   (c) Did you discuss any potential negative societal impacts of your work? [No] No potential negative societal impacts were identified.
   (d) Have you read the ethics review guidelines and ensured that your paper conforms to them? [Yes]
2. If you are including theoretical results...
   (a) Did you state the full set of assumptions of all theoretical results? [N/A] Only include experimental results.
   (b) Did you include complete proofs of all theoretical results? [N/A] Only include experimental results.
3. If you ran experiments...

(a) Did you include the code, data, and instructions needed to reproduce the main experimental results (either in the supplemental material or as a URL)? [No] Code is provided, ADNI data is public, but eye gaze dataset is private (from authors' institution).

(b) Did you specify all the training details (e.g., data splits, hyperparameters, how they were chosen)? [Yes] See section 4.4.

(c) Did you report error bars (e.g., with respect to the random seed after running experiments multiple times)? [Yes] Standard deviations of results are on Tab. 3 and Tab. 4.

(d) Did you include the total amount of compute and the type of resources used (e.g., type of GPUs, internal cluster, or cloud provider)? [Yes] See section 4.4. Type of GPU depends on Google's allocation policy, thus not always the same.

4. If you are using existing assets (e.g., code, data, models) or curating/releasing new assets...

(a) If your work uses existing assets, did you cite the creators? [Yes] See section 3.

(b) Did you mention the license of the assets? [No] One dataset is public and the other is from authors own institution.

(c) Did you include any new assets either in the supplemental material or as a URL? [Yes] A URL with the code is mentioned in section 4.4.

(d) Did you discuss whether and how consent was obtained from people whose data you're using/curating? [No] ADNI data is public and eye-gaze is from authors own institution.

(e) Did you discuss whether the data you are using/curating contains personally identifiable information or offensive content? [No] Data used does not have any personally identifiable information or offensive content.

5. If you used crowdsourcing or conducted research with human subjects...

(a) Did you include the full text of instructions given to participants and screenshots, if applicable? [N/A] Data from human subjects was collected by other authors and institutions. These stakeholders provid their data for others to use. The authors of this paper did not conduct research with human subjects specifically for this paper.

(b) Did you describe any potential participant risks, with links to Institutional Review Board (IRB) approvals, if applicable? [N/A]

(c) Did you include the estimated hourly wage paid to participants and the total amount spent on participant compensation? [N/A]